Evidence for 15O + α resonance structures in 19Ne via direct measurement

Torresi, Domenico; Wheldon, Carl; Kokalova Wheldon, Tzanka; Bailey, Sam; Boiano, A.; Boiano, C.; Fisichella, M.; Mazzocco, M.; Parascandolo, C.; Pierroutsakou, D.; Strano, E.; Zadro, M.; Cavallaro, M.; Cherubini, S.; Curtis, Neil; Di Pietro, A.; Fernández Garcia, J. P.; Figuera, P.; Glodariu, T.; Grbosz, J.

DOI:
10.1103/PhysRevC.96.044317

Evidence for ^{15}O+α resonance structures in ^{19}Ne via direct measurement

D. Torresi,[1,2,3] C. Wheldon,[1,*] Tz. Kokalova,[1] S. Bailey,[1] A. Boiano,[4] C. Boiano,[5] M. Fisichella,[2] M. Mazzocco,[6,7] C. Parascandolo,[4] D. Pierroutsakou,[4] E. Strano,[6,7] M. Zadro,[8] M. Cavallaro,[2] S. Cherubini,[2,3] N. Curtis,[1] A. Di Pietro,[2] J.P. Fernández Garcia,[2] P. Figuera,[2] T. Glodariu,[9] J. Gręboszl,[10] M. La Cognata,[2] M. La Commara,[4] M. Lattuada,[2,3] D. Mengoni,[11] R.G. Pizzone,[7,2] C. Signorini,[11] C. Stefanini,[6] L. Stroe,[9] and C. Spitaleri[2,3]

[1] *School of Physics and Astronomy, University of Birmingham, Edgbaston, Birmingham B15 2TT, United Kingdom*
[2] *INFN-Laboratori Nazionali del Sud, Via S. Sofia 62 Catania, Italy*
[3] *Dipartimento di Fisica e Astronomia Universitá di Catania, Via S. Sofia 64, I-95123 Catania, Italy*
[4] *INFN-Sezione di Napoli, Via Cinthia, I-80126 Napoli, Italy*
[5] *INFN-Sezione di Milano, Via Celoria 16, I-20133 Milano, Italy*
[6] *INFN-Sezione di Padova, Via F. Marzolo 8, I-35131 Padova, Italy*
[7] *Dipartimento di Fisica e Astronomia, Universitá di Padova, Via F. Marzolo 8, I-35131 Padova, Italy*
[8] *Ruđer Bošković Institute, Bijenička cesta 54, 10000 Zagreb, Croatia*
[9] *NIPNE (IFIN-HH), 30 Reactorului Street, 077125 Magurele, Romania*
[10] *Institute of Nuclear Physics, Polish Academy of Sciences, 31-342 Krakow, Poland*
[11] *INFN-Laboratori Nazionali di Legnaro, Viale dell'Universitá 2, I-35020 Legnaro, Italy*

(Dated: October 11, 2017)

States in the astrophysically important ^{19}Ne nucleus have been populated directly using the ^{15}O(α, α)^{15}O reaction with a radioactive ^{15}O beam. Due to the challenges involved, this represents the first such ^{15}O measurement with high resolution and the first dedicated to exploring the cluster structure. This measurement comprises three experiments: the first to develop the ^{15}O radioactive beam, the second the resonant scattering study and the third to measure the precise energy loss of O ions in ^{4}He to reduce systematic uncertainties. The results show evidence for ^{15}O+α cluster structure which could explain earlier results pointing to the increased α branching ratio in the astrophysical reaction rate for high-spin near-threshold resonances. Absolute differential cross sections have been measured. Additionally, spins, parities and partial decay widths, essential for nuclear reaction-rate calculations, have been extracted using an R-matrix analysis.

PACS numbers: 21.60.Gx, 25.60.-t, 25.60.Bx, 27.20.+n

INTRODUCTION

One of the nuclear reactions with fundamental significance for understanding the on-set of the thermonuclear runaway on the surface of accreting neutron stars or X-ray bursts is ^{15}O(α,γ)^{19}Ne. This reaction, though not fully elucidated, is thought to trigger the colossal release of energy in accreting neutron stars that is observed as X-ray bursts [1–3], marking the break out from the hot-CNO cycles and the commencement of rapid proton capture. As a result, the structure of the low-lying energy levels close to the ^{15}O+α threshold in ^{19}Ne [4, 5] (S_α=3.528 MeV [6]) is extremely important. Any enhancement of – or reduction in – the (α,γ) rate has significant consequences for energy production in the universe.

A second crucial role is played by the ^{19}Ne excitation region around the proton threshold (S_p=6.411 MeV [6]) due to its importance for the destruction of the key radionuclide ^{18}F [7–9] — this isotope survives long enough to provide evidence of nucleosynthesis via observable γ-ray emission. Destruction is via proton-unbound states in ^{19}Ne through the reaction ^{18}F(p,α)^{15}O.

From a nuclear structure perspective it is well known that heavier neon isotopes exhibit strong α clustering even in the ground states with ^{20}Ne [10–12] and ^{21}Ne [13, 14] being two of the best examples known to date. Thus, the question arises about the possibility of α clustering in ^{19}Ne and whether similar states above the α and proton thresholds exhibit ^{15}O+α structure, and if so, to what extent. This letter reports on the direct measurement of the ^{15}O+α reaction using resonant scattering [15] with a radioactive ^{15}O beam developed specifically for this study. In this way the *rotations* of the near α-threshold states were populated, and thereby their underlying structure established.

The method, as implemented here, enables α strength to be measured *directly* via elastic scattering across a large excitation-energy range using one beam energy. The nature of the technique makes it ideally suited to use with low-intensity, large-energy-profile beams. Previously, there has been a single attempt using an ^{15}O beam and a small gas-cell where only one resonance was populated with low resolution [16].

In Thick Target in Inverse Kinematics (TTIK) resonant scattering [15], a low-intensity beam is incident on an extended gas target. As the projectiles slow down in the gas, elastic scattering reactions across a

* Corresponding author: c.wheldon@bham.ac.uk

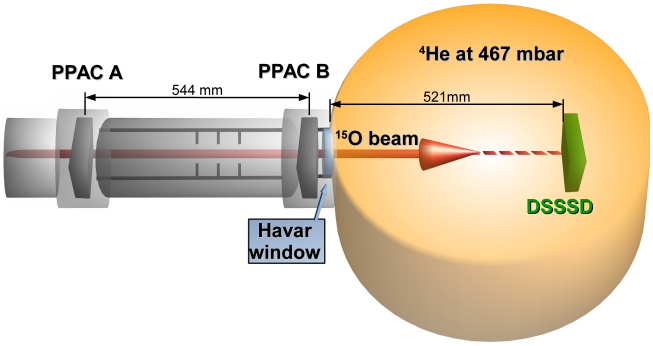

FIG. 1. (color online) Schematic (not to scale) of the experimental apparatus. The detection system consisted of a DSSSD and two PPACs required for the Time-Of-Flight measurement and beam tracking.

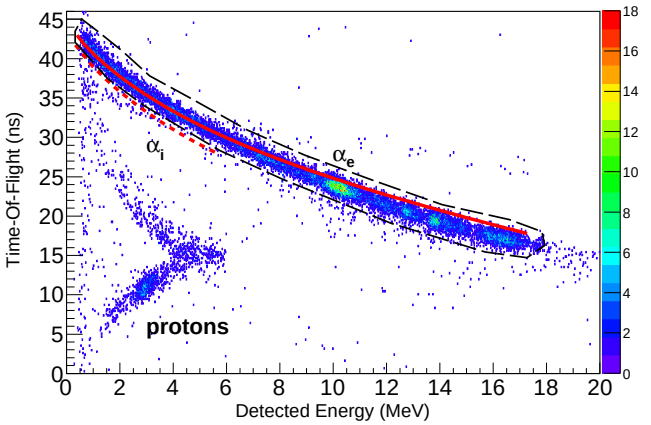

FIG. 2. (color online) A plot of detected energy versus TOF. Alpha particles originating from elastic scattering (and selected for further analysis) correspond to the locus inside the black long-dashed contour. The corresponding simulated distribution is indicated by the red continuous line. The red short-dashed line corresponds to α particles originating from inelastic scattering, demonstrating that events from this process can be excluded from the analysis, but in this instance, have not been observed. The intensities are given by the heat-map color scale. *Note, that as inelastic excitation reduces the available kinetic energy, these reactions take place in the gas closer to the window for the same detected α energy. Since the α particles travel faster than the ^{15}O ions, this reduced ^{15}O flight path leads to a shorter TOF, giving the position of the inelastic locus as shown here.*

wide range of center-of-mass (*com*) energies can take place (corresponding to a range of depths within the gas). The pressure of the gas is tuned such that the beam completely stops in the gas, allowing a detector to be placed at 0°, *i.e.* on the beam axis. The elastic scattering leads to energetic light particles which, due to their lower-rate of energy loss, can traverse the gas and be recorded by the detector. The result is that low-intensity beams can be used to measure large-range excitation functions in one measurement with one initial beam energy. In the current work the technique is refined by using Time-Of-Flight (TOF) [17] to remove contributions from processes other than elastic scattering [18]. This is the first resonant scattering experiment at the EXOTIC facility [19, 20].

EXPERIMENTAL TECHNIQUE

The 28.5 MeV ^{15}O radioactive ion beam was produced with the EXOTIC facility [19, 20] at the Laboratori Nazionali di Legnaro (LNL, Italy) by means of the in-flight technique via the $p(^{15}\mathrm{N},^{15}\mathrm{O})n$ reaction. A primary 80 MeV $^{15}\mathrm{N}^{5+}$ beam was delivered by the LNL-XTU tandem Van de Graaff accelerator and impinged on a H_2 gas target at a pressure of 1 bar and cooled with liquid nitrogen, corresponding to an equivalent target thickness of about 1.35 mg/cm^2 of H_2.

The ^{15}O beam was selected and purified from the scattered primary ^{15}N beam and other contaminant nuclei by tuning the 30°-bending magnet, Wien-filter and six quadrupole lenses of the EXOTIC facility. Two parallel plate avalanche counters (PPACs) [21] were placed downstream prior to the beam entering the scattering chamber. The PPACs were utilized as counters and for timing and on-line monitoring of the ^{15}O beam (PPAC A predominantly during tuning and as a reference/check for PPAC B). Finally, the ^{15}O beam crossed a 2.2 μm thick Havar window that separated the scattering chamber filled with ^{4}He gas at a pressure of 467 mbar from the high vacuum beam line (see Fig. 1). The ^{4}He gas pressure and temperature were continuously monitored and did not change appreciably during the experiment. The ^{15}O beam intensity was typically in the range 1-2$\times10^4$ particles/s with ≈99% purity. (*Aside:* development of the ^{15}O beam was carried out by the present authors approximately 1 year prior to the experiment and is reported in Ref. [22].)

The apparatus for detecting the elastically scattered light charged particles, illustrated in Fig. 1, consisted of one 300 μm double-sided silicon strip detector (DSSSD) from the EXPADES detector array [21], capable of stopping α particles upto 24 MeV. The 6.4×6.4 cm^2 0° DSSSD was segmented here into 16 strips — orthogonal on each face — yielding 256 effective pixels. The angular acceptance of this 0° detector is 3.5° in the laboratory frame (6.5° *com*) for scattering events occurring at the entrance of the chamber and 6.6° in the laboratory frame (14.5° *com*) for those events occurring at a distance of approximately 310 mm from the window.

ANALYSIS

The identification of α-particles was performed by measuring the TOF between an ^{15}O particle crossing PPAC B and the detection of the recoiling α-particle in the silicon detector, as done, for example, in Ref. [17].

In the present experiment the TOF measurements also allowed the discrimination between elastic and inelastic scattering [18]. The identification plot, Fig. 2, shows TOF versus detected α-particle energy. The calculation for α-particles that are elastically (upper solid red line) or inelastically scattered (lower short-dashed red line) are superimposed on the experimental data. (Inelastic scattering would lead to an excited $^{15}O^*$ recoil, the first excited state of which lies at 5.183 MeV [23].) As can be seen, there is no evidence of inelastic events in the data. Clean (proton- and inelastic-free) elastic scattering events were selected by a graphical cut (black long-dashed line) in Fig. 2. Additionally, the information from PPAC B, the measured efficiency of which is ≈90%, was used to count the beam particles entering the scattering chamber in order to obtain the absolute elastic scattering differential cross sections.

Once the elastically scattered α-particles are selected it is possible to transform the detected α-particle energy into center-of-mass energy, E_{com}, providing the stopping powers of ^{4}He and ^{15}O in ^{4}He are known. Knowledge of the stopping power for the incident beam in ^{4}He gas is critical in this method, since any inaccuracies generate distortion in the deduced excitation function as shown in Fig. 2 of Ref. [24]. For this reason instead of using the stopping power calculated with codes such as SRIM [25] *etc.*, which can introduce systematic errors as large as 15%, the stopping power for ^{16}O in ^{4}He has been measured [26]. This enabled the associated values for ^{15}O in ^{4}He to be deduced as the electronic stopping power depends only on the atomic features of the ion. This scaling from a known isotope only requires the velocity change arising from the mass difference which can be easily calculated. To emphasize the importance of this correction, an interaction taking place 200 mm after the window leads to an energy loss for ^{15}O of 16.9 MeV (28.5→11.6 MeV) and for an elastically scattered α produced at the same position, the energy loss is 2.1 MeV (7.7→5.6 MeV).

The resulting elastic scattering excitation function is shown in Fig. 3. The energy resolution of (FWHM) ≈20-30 keV in the *com* frame (corresponding to FWHM≈50 keV in the laboratory frame) has been found, from Monte-Carlo simulations [27], to be approximately constant over the measured energy range. The resolution is an effect of energy and angular beam spread and also includes intrinsic detector and electronics contributions.

R-Matrix analysis

In order to extract widths, partial decay branches, energies and spins for the states, the *R*-matrix method was used which solves the coupled Schrödinger equations for several reaction channels in order to fully describe the properties of the populated levels. A comprehensive description can be found in Ref. [28].

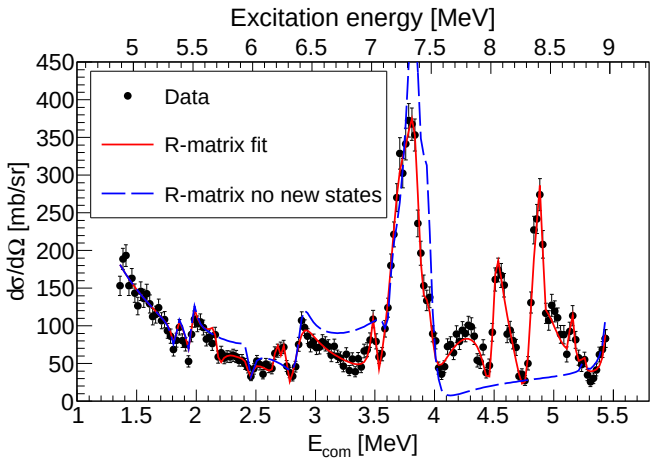

FIG. 3. (color online) Excitation function for ^{19}Ne at 0°. The data points from the current work are overlaid by the *R*-matrix fit (solid red line). The fit without the newly observed levels is shown for comparison (dashed blue line). See text and Table I for details.

A full *R*-matrix fit was performed using AZURE2 [29] for 0° (θ_{com}=180°). As a starting point for the fit, spins and energies of states from the mirror nucleus, ^{19}F [30], were used; a powerful technique, with a good agreement between the energy levels in each nucleus. However, it should be noted that the absence of information at angles away from 0° naturally leads to some uncertainty in the final spin assignments. This has been explored by varying the spins and parities of the states systematically and comparing the goodness of fit. As a result, some states have two possible assignments, though there is the possibility of an alternative solution if the parameters of many states were to be different. However, the agreement obtained to known states in both ^{19}F and ^{19}Ne increases confidence in the assignments.

The two open particle-decay channels were incorporated into the fit (as radiative capture is negligible at these excitation energies): $^{15}O(1/2^-) + \alpha(0^+)$ and $^{18}F(1^+) + p(1/2^+)$, with channel radii for the i^{th} decay channel, $r_i = r_0(A_{recoil}^{\frac{1}{3}} + A_i^{\frac{1}{3}})$ fm and r_0=1.4 fm. The results of the fit (Fig. 3) are tabulated in Table I. An experimental resolution in the laboratory frame of FWHM=50 keV (σ=21 keV) has been included in the fit. The final χ^2/d.o.f. is 1.38 (for 125 d.o.f.).

The formal definition of the reduced widths *on-resonance*, γ_i^2, is

$$\gamma_i^2 = \frac{\Gamma_i}{2P_i} = \Gamma_{tot.}\frac{\Gamma_i}{\Gamma_{tot.}}\frac{\left[F_l^2(k_i r_i) + G_l^2(k_i r_i)\right]}{2k_i r_i}, \qquad (1)$$

where the barrier penetrabilities, P_i, dependent on the *regular*, $F_l(k_i r_i)$, and *irregular*, $G_l(k_i r_i)$, Coulomb wave functions, are removed. The orbital angular momentum carried by the decay particle is denoted by l; k_i are the wave numbers and $\Gamma_i/\Gamma_{tot.}$ are the decay branching ratios. In AZURE2, the definition of γ_i^2 takes into account, via the Coulomb shift, the changing penetrabilities as a

TABLE I. The energy levels of ^{19}Ne from the present R-matrix fit, compared with candidate states taken from the compilation for ^{19}Ne [30] and more recent references where indicated. Statistical errors arising from the R-matrix fit are given in parentheses, but for the energies in the first column there is an additional systematic uncertainty of ≈50 keV. Energies in **bold** are newly observed in the present work. Note that only *measured* widths from the literature are listed for ^{19}Ne. See text for details. Where multiple assignments are given, θ^2_α corresponds to the first. Grey shading highlights the new information obtained in the current work. Additionally, the properties of corresponding levels in ^{19}F [30] are quoted in the final three columns.

^{19}Ne current work		^{19}Ne literature		^{19}Ne current work				^{19}Ne literature			^{19}F literature		
E_x (MeV)	I^π [i]	E_x (MeV)	I^π	Γ_α (keV)	Γ_p (keV)	$\Gamma_{tot.}$ (keV)	θ^2_α	Γ_α (keV)	Γ_p (keV)	$\Gamma_{tot.}$ (keV)	E_x (MeV)	I^π [i]	$\Gamma_{tot.}$ (keV)
5.359(6)	$1/2^+$	5.351(6)	$1/2^+$	10(3)		10(3)	0.61(10)	3.2(16)[f]			5.337(2)	$1/2^{(+)}$	≥4.7 eV
5.487(4)	$3/2^+$	5.463(20)	$3/2^+$	9(2)		9(2)	0.39(4)				5.501(2)	$3/2^+$	4
5.704(8)	$5/2^-$			29(6)		29(6)	0.98(10)				5.621(1)	$5/2^-$	>0.36 eV
5.983(9)	$3/2^-$	6.013(7)	$(3/2^-)$	21(8)		21(8)	0.42(8)				6.088(1)	$3/2^-$	4
6.197(8)	$1/2^-$ $(1/2^+)$			16(5)		16(7)	0.14(2)				6.255(1)	$1/2^+$	8
6.279(2)	$5/2^+$	6.288(7)	$(1/2, 3/2, 5/2)^+$	6(2)		6(2)	0.27(5)				6.282(2)	$5/2^+$	2.4
6.395(5)	$1/2^-$	6.437(9)	$(1/2^-)$	181(58)		181(58)	0.44(7)	216(19)[g]			6.536	$1/2^-$	245
$S_p(^{19}\text{Ne}) = 6.410$ MeV													
7.030(4)	$7/2^+$			12(3)		12(3)	0.17(2)				7.114(6)	$7/2^+$	32
7.153(9)	$3/2^+$	7.076[b]/7.238[a]	$3/2^+$	233(44)	19(14)	252(39)	0.39(4)	28(3)[c]	14(2)[c]		7.262(2)	$3/2^+$	<6
7.378(7)	$7/2^+$	7.42[b]	$7/2^+$	121(9)		121(9)	0.44(2)	71(11)[h]			7.560(10)	$7/2^+$	<90
7.469(7)	$5/2^+$	7.500(3)[a,c,d]	$5/2^+$	83(17)		83(17)	0.34(3)			17(7)[d,g]	7.540(1)	$5/2^+$	0.16
7.568(27)	$(3/2^+)$ $(1/2^+)$	7.616(16)[d]	$3/2^+$	774(144)		774(144)	0.57(5)			21(10)[d]	7.661(9)	$3/2^+$	2.2 eV
8.022(4)	$9/2^+$			64(10)		64(10)	0.84(7)				7.929(3)	$7/2^+$,$9/2$	—
8.223(7)	$5/2^+$			377(34)		377(34)	0.51(2)				8.199(1)	$(5/2^+)$	<0.8
8.428(2)	$13/2^-$ $(11/2^+)$			4(1)		4(1)	0.31(4)				8.288(2)	$13/2^-$	<1
8.680(1)	$(9/2^-)$ $(7/2^-)$			3(1)		3(1)	0.054(6)				8.864(4)	$\leq 7/2$	≈1
(8.790)	$(11/2^{-/+})$	8.920(9)	$(11/2^-)$	4(1)		4(1)	0.10(3)				8.953(3)	$11/2^-$	≈1

[a] ^{18}F(p,α)^{15}O [34]; [b] ^{18}F(p,p)^{18}F [35, 36]; [c] ^{18}F(p,p)^{18}F & ^{18}F(p,α)^{15}O [37]; [d] Inelastic scattering $p(^{19}\text{Ne},p)^{19}$Ne [38]; [e] ^{20}Ne(p,d)^{19}Ne [7]; [f] Ref. [16]; [g] ^{19}F(^{3}He,t)^{19}Ne Ref. [39]; [h] Ref. [40]. [i] See text for details.

function of energy due to the finite resonance widths. However, due to the narrowness of the resonances observed in the current work the reduced widths obtained from the R-matrix fit will approximate to those given by Eqn.1. The ratio, θ^2_i, of the reduced width to the first Wigner sum rule, γ^2_{Wi} [31, 32] (also called the Wigner single-particle limit) gives a measure of the extent of preformation or clustering for each decay channel. This ratio can be expressed as

$$\theta^2_i = \frac{\gamma^2_i}{\gamma^2_{Wi}} = \Gamma_i \frac{2\mu_i r_i^2 \left[F_l^2(k_i r_i) + G_l^2(k_i r_i)\right]}{6\hbar^2 k_i r_i}\,, \qquad (2)$$

as formulated by Sanders *et al.* [33], where μ_i is the reduced mass of the recoil and decay particles. Values of $\theta^2_i > 0.1$ are taken to indicate significant clustering. Similarly, the physical requirement that $\theta^2_\alpha < 1$ can be used to constrain branching ratios and/or spin-parity assignments, as the penetrabilities, P_i, decrease with increasing l. Therefore, an upper limit on the reduced width can be obtained which in turn enables possible spin assignments of a state to be restricted. The latter is via the conservation of angular momentum vectors, $\underline{I}_{^{19}\text{Ne}^*} - \underline{l}_\alpha = \underline{I}_\alpha + \underline{I}_{^{15}\text{O}_{gs}}$ which, using the known ground-state spins for ^{15}O and α reduces to selection rules of

$$\underline{I}_{^{19}\text{Ne}^*} = \underline{l}_\alpha \pm 1/2 \;\text{ and }\; \pi_{^{19}\text{Ne}^*} = (-1)^l \otimes (-1)\,. \qquad (3)$$

The results of the R-matrix and width analysis are summarized in Table I.

RESULTS AND INTERPRETATION

The absolute R-matrix cross sections (red solid line of Fig. 3) are within 4% of the values obtained independently from the experimental data via measurement of the beam current using PPAC B (data of Fig. 3). As can be seen from Table I, many of the levels compare well with previously observed states and the most likely candidates from the literature based on spin, parity and energy are given for comparison. Those marked in bold in Table I are newly observed in the current work, *i.e.* no comparable state is known in the literature; two of these lie below the proton threshold. Furthermore, very little information exists in the literature for the widths – both total and partial – of states in the excitation region populated here. This paucity has been noted by Tan *et al.* [41]. Where information does exist, it is often based on the reduced width of the equivalent mirror states in ^{19}F. However, the physical properties of states are quoted here only where measured data exist to provide a like-for-like comparison. Also note that only the 7.153 MeV level has a non-negligible proton width of 19(14) keV, consistent with the literature value of 14(2) keV [37]. To further discuss the results, the final three columns of Table I contain the excitation energies, spins and parities and total widths for corresponding states in the mirror partner ^{19}F [30].

The spins and parities obtained here agree well with previous results where available, in several cases support-

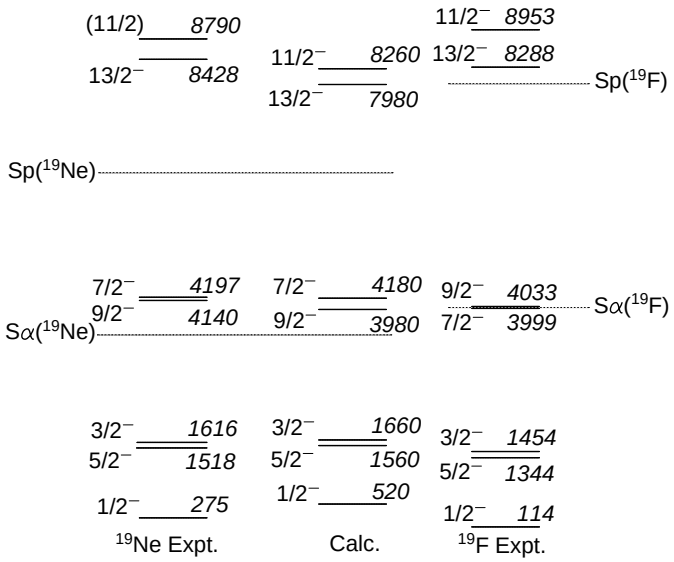

FIG. 4. Energy levels of ^{19}Ne corresponding to the ^{15}O+α rotational bands. The levels predicted in Ref. [42] (in the middle) are compared with the levels experimentally measured in the present work and Ref. [30] (on the left) and to the corresponding ^{15}N+α negative parity band in ^{19}F (on the right) [30, 43].

ing previous tentative assignments, *e.g.* for the 5.983, 6.279 and 6.395 MeV levels. The large energy difference between the tentatively observed 8.790 MeV state and the 8.920 MeV literature value implies that these could be different levels. For the states populated only one is observed to have a non-negligible proton decay – the 7.153 MeV state. This is due to the selectivity of the reaction. The resonance technique used here, by its nature selectively populates states which undergo disintegration via α decay, once again highlighting the usefulness of making this direct measurement over indirect techniques which can suppress states with α character. It should be noted that the 8.814 MeV state has large uncertainties on both the width and energy and as such remains tentative, since additional components from overlapping levels cannot be resolved. In part, this is due to the full energy not being fully inside the explored excitation energy range. As a result, no associated mirror state is included.

Partial widths for all the states have been extracted from the R-matrix fit, which for most of the levels is the first such measurement. Note that due to the possibility of states with small natural widths occurring, the θ_α^2 values in Table I could, in such cases, represent upper limits. Where width data have been reported there is qualitative agreement with the exception of the 7.153 MeV α width and 7.568 MeV total width. For the former, the uncertainty is large, perhaps indicating an additional juxtaposed α-decaying resonance. For the 7.568 MeV state, either a resonance different to that reported in the literature has been populated or there is an additional, unidentified level at a similar excitation energy. The relatively large uncertainty on the observed energy ($\pm$27 keV) could be indicative of this latter scenario.

In terms of mirror structure, there is a good correspondence between the newly observed levels in ^{19}Ne and their counterparts in ^{19}F, with differences been in general $<$200 keV and in most cases $<$100 keV.

For near-threshold resonances knowledge of the partial decay widths (as well as energies) are needed as these affect reaction-rate calculations, so the large number of states for which α-width data have been obtained represents a key result for the destruction of ^{18}F via ^{18}F(p,α)^{15}O.

In terms of the underlying structure, recently Otani *et al.* [42] have performed calculations of ^{15}O+α rotational bands in a simple potential model calculation using the well known ^{16}O+α cluster band configurations and ^{15}N+α elastic scattering data. The analog states of the ^{16}O+α 0^+, 2^+, 4^+ and 6^+ rotational sequence in ^{20}Ne leads to doublets (one favored and one unfavored signature) for all but the 0^+ state, resulting in ^{19}Ne levels with spins of $^1/_2{}^- \rightarrow {}^{17}/_2{}^-$. Table II and Fig. 4 summarize both the calculated and experimental levels. It can be seen that the newly observed $^{13}/_2{}^-$ level at 8.428 MeV is very close to the predicted rotational level. Though not a unique assignment in this case ($^{11}/_2{}^+$ yields a fit comparable to that of Fig. 3) there is a corresponding $^{13}/_2{}^-$ level in ^{19}F at 8.288 MeV. Previously no $^{13}/_2{}^-$ level was known in ^{19}Ne in this energy regime. Additionally, the spin of the $^{11}/_2{}^-$ state at 8.790 MeV in the present study is consistent with that given in Ref. [30], though there is a 200 keV energy difference possibly indicating this may be a previously unobserved level. Despite being relatively weak, this resonance is only reproduced well via an $^{11}/_2$ assignment, but the parity remains uncertain. However, looking across the entire band, the agreement between calculated and measured excitation energy is good, albeit tentative. Otani and coworkers further predict the $^{17}/_2{}^-$ and $^{15}/_2{}^-$ levels at 14.05 and 14.44 MeV respectively, as analogs of the 8^+ ^{16}O+α state in ^{20}Ne.

In order to further explore the structure of the observed states, the reduced-width-to-Wigner limit, θ_α^2 (Eq. 2), was examined for the α-decay branches. A significant number of the observed levels have a relatively large ratio to the Wigner limit, above the nominal 10% that is used to indicate significant α preformation. This is as expected due to the predisposition of the reaction for populating states with ^{15}O+α character.

Focusing on the predicted ^{15}O+α cluster band members (Table II), it can be seen that θ_α^2 values obtained here are the first values established from measurements. It was noted by Tan *et al.* [41] that the upper limit they obtained for the branching ratio of the 4.14 MeV level of $1.2(0.5)\times10^{-3}$ was unexpectedly large and might indicate a possible α-cluster configuration. This gives it a more significant role in the hot CNO break out – dominating in some temperature regimes. (Note that part or all of the α strength could be from the 4.197 MeV state in

TABLE II. Comparison of the calculated and measured α+^{15}O rotational levels. Lines shaded grey represent the new information obtained in the current work.

Expt.			Calc.[a]	
E_x (MeV)	I^π	θ_α^2	E_x (MeV)	I^π
0.27509(13)[b]	$1/2^-$[a]	(bound)	0.52	$1/2^-$
1.51756(3)[b]	$5/2^-$[a]	(bound)	1.56	$5/2^-$
1.6156(5)[b]	$3/2^-$[a]	(bound)	1.66	$3/2^-$
4.140(4)[b]	$(9/2^-)$	$\leq$1[c]	3.98	$9/2^-$
4.197(2)[b]	$(7/2^-)$	$\leq$0.1[c]	4.18	$7/2^-$
8.428(2)[d]	$(13/2^-)$[b]	0.31(4)[d]	7.98	$13/2^-$
(8.790)[d]	$(11/2^{-/+})$[b]	0.10(3)[d]	8.26	$11/2^-$
14.2(3)[b]	—	—	13.67	$17/2^-$
14.5(3)[b]	—	—	14.26	$15/2^-$

[a]There is an uncertainty of ≈50 keV on the calculated energies for $9/2^-$ and above, from extracting the values from Fig. 3 of Ref. [42]. [b]Ref. [30]. [c]Based on the level properties given by Tan *et al.* [41]. [d]Present work.

Ref. [41] but both states disintegrate via l_α=4, implying similar penetrabilities.) The present work is compatible with a cluster interpretation for the 4.14 MeV level. For the levels in the predicted α cluster band (Table II), the $9/2^-$:$7/2^-$ pair exhibits the same behavior as the newly measured $13/2^-$:($11/2^-$) states (though the second is tentative), with the favored state having the larger α-width-to-Wigner ratio in each instance, but all four levels possessing significant ratios, *i.e.* >0.1.

Comparing to the band structure in ^{19}F as shown in Fig. 4, the similarities are, as expected, striking and supports the reversal (compared to column one of Fig. 4) of the $9/2^-$:$7/2^-$ assignments in ^{19}Ne as favored by Tan *et al.* [41]. The majority of the states in the mirror band are either below or at threshold such that θ_α values cannot be extracted. However, for the $13/2^-$ and $11/2^-$ states upper limits based on $\Gamma_\alpha/\Gamma_{tot.}\leq$1 yield ratios to the Wigner limit of $\leq$6% and $\leq$2% respectively, tentatively indicating less clustering than observed in ^{19}Ne and suggests that ^{15}O could be a more robust core than ^{15}N.

This study has shown that by identifying and studying the α+^{15}O configuration significantly above threshold, the nature of associated states near and below threshold can be elucidated.

It is also noteworthy that the majority of levels observed in the current work have large α partial decay widths with most of the θ_α^2 values corresponding to a significant fraction of the Wigner limit. This further confirms the selectivity of this technique for populating states with manifest α character.

CONCLUSION

In summary, the challenging direct measurement of states in ^{19}Ne via the resonant elastic scattering of a radioactive ^{15}O beam on an extended ^{4}He gas target has been achieved across a wide energy range for the first time. Levels in the 5.3 – 8.8 MeV excitation-energy region have been explored, with a significant number (at least seven) newly observed in the present work. Additionally, partial widths have been extracted for the observed levels, the majority (thirteen) for the first time. Reliable cross sections have been measured across the full range of levels populated representing important input to reaction-rate models.

Evidence for the predicted α+^{15}O rotational structure has been obtained. Such an enhanced α structure could explain the increased role played by some levels in the astrophysical ^{15}O(α,γ)^{19}Ne reaction that is important for break out from the hot CNO cycles and, therefore, for X-ray bursts due to the subsequent onset of rapid proton capture reactions. Additionally, levels have been newly identified close to the proton threshold, which may have consequences for the destruction of ^{18}F, though more work is needed to establish the magnitude of proton widths in this energy region.

ACKNOWLEDGMENTS

S. Pirrie is thanked for commenting on the manuscript. The UK STFC is acknowledged for providing funding under grant number ST/L005751/1. MZ was partially supported by the Croatian Science Foundation under Project No. 7194. This work has received funding from the European Union's Horizon 2020 research and innovation programme under the Marie Skłodowska-Curie grant agreement No 659744.

[1] M. Wiescher *et al.*, Prog. Part. and Nucl. Phys. **59**, 51 (2007).
[2] M. Wiescher, J. Görres, E. Uberseder, G. Imbriani and M. Pignatari, Annu. Rev. Nucl. Part. Sci. **60**, 381 (2010).
[3] Anuj Parikh, Jordi José, Fermín Moreno and Christian Iliadis Astrophysical J. Supp. **178**, 110 (2008).
[4] M. Thoennessen, Atomic Data and Nucl. Data Tables **98** (2012) 43.
[5] J.G. Fox, E.C. Creutz, M.G. White, L.A. Delsasso, Phys. Rev. **55** (1939) 1106.
[6] M. Wang, G. Audi, A.H. Wapstra, F.G. Kondev, M. MacCormick, X. Xu, B. Pfeiffer, Chin. Phys. C **36**, 1603 (2012).
[7] D.W. Bardayan *et al.*, Phys. Lett. B **751**, 311 (2015).
[8] A.M. Laird *et al.*, Phys. Rev. Lett. **110**, 032502 (2013).
[9] A.S. Adekola *et al.*, Phys. Rev. C **84**, 054611 (2011).
[10] W. von Oertzen, Eur. Phys. J. A **11**, 403 (2001).
[11] Martin Freer, Rep. Prog. Phys. **70**, 2149 (2007).
[12] W. von Oertzen, Martin Freer and Yoshiko Kanada-En'yo, Phys. Rep. **432** (2006) 43.
[13] S. Thummerer *et al.*, J. Phys. G **29**, 509 (2003).
[14] C. Wheldon *et al.*, Eur. Phys. J. A **26**, 321 (2005).
[15] K.P. Artemov *et al.*, Sov. J. Nucl. Phys. **52**, 634 (1990).

[16] F. Vanderbist *et al.*, Eur. Phys. J. A **27**, 183 (2006).
[17] C. Fu *et al.*, Phys. Rev. C **76**, 021603(R) (2007) and Phys. Rev. C **77**, 064314 (2008).
[18] D. Torresi *et al.*, Int. J. Mod. Phys. E **20**, 1026 (2011).
[19] V.Z. Maidikov *et al.*, Nucl. Phys. A **746**, 389c (2004).
[20] M. Mazzocco *et al.*, Nucl. Instr. and Meth. in Phys. Res. B **317**, 223 (2013).
[21] D. Pierroutsakou *et al.*, submitted to Nucl. Instr. and Meth. in Phys. Res. A.
[22] D. Torresi, C. Wheldon *et al.*, LNL Annual Report (2014) p19, see *http://www.lnl.infn.it/∼annrep/read_ar/2014/contributions/pdfs/019_A_61_A056.pdf.*
[23] F. Ajzenberg-Selove, Nucl. Phys. A **523**, 1 (1991).
[24] M. Zadro *et al.*, Nucl. Instr. and Meth. in Phys. Res. B **259**, 836 (2007).
[25] J.F. Ziegler, Nucl. Instr. and Meth. in Phys. Res. B **219-220**, 1027 (2004).
[26] D. Torresi, D. Carbone, M. Cavallaro, A. Di Pietro, J.P. Fernández Garcia, P. Figuera, M. Fisichella, M. Lattuada, M. Zadro, Nucl. Instr. and Meth. in Phys. Res. B **389-390**, 1 (2016).
[27] N. Curtis and J. Walshe, Nucl. Instr. and Meth. in Phys. Res. A **797**, 44 (2015).
[28] A,M. Lane and R.G. Thomas, Reviews of Modern Physics **30**, 257 (1958).
[29] R.E. Azuma *et al.*, Phys. Rev. C **81**, 045805 (2010).
[30] D.R. Tilley, H.R. Weller, C.M. Cheves, R.M. Chasteler, Nucl. Phys A **595** (1995) 1.
[31] R. Nilson, W.K. Jentschke, G.R. Briggs, R.O. Kerman and J.N. Snyder, Phys. Rev. **109**, 850 (1958).
[32] T. Teichmann and E.P. Wigner, Phys. Rev. **87**, 123 (1952).
[33] S.J. Sanders, L.M. Martz and P.D. Parker, Phys. Rev. **C 20**, 1743 (1979).
[34] C.E. Beer *et al.*, Phys. Rev. C **83**, 042801(R) (2011).
[35] D.W. Bardayan, J.C. Blackmon, J. Gómez del Campo, R.L. Kozub, J.F. Liang, Z. Ma, L. Sahin, D. Shapira and M.S. Smith, Phys. Rev. C **70**, 015804 (2004).
[36] H.T. Fortune, A. Lacaze and R. Sherr, Phys. Rev. C **82**, 034312 (2010).
[37] A. St. J. Murphy *et al.*, Phys. Rev. C **79**, 058801 (2009).
[38] J.C. Dalouzy *et al.*, Phys. Rev. Lett. **102**, 162503 (2009).
[39] S. Utku *et al.*, Phys. Rev. C **57**, 2731 (1998).
[40] C.D. Nesaraja, N. Shu, D.W. Bardayan, J.C. Blackmon, Y.S. Chen, R.L. Kozub and M.S. Smith, Phys. Rev. C **75**, 055809 (2007).
[41] W.P. Tan *et al.*, Phys. Rev. C **79**, 055805 (2009).
[42] R. Otani, R. Kageyama, M. Iwasaki, M. Kudo, M. Tomita and M. Ito, Phys. Rev. C **90**, 034316 (2014).
[43] T. Sakuda and F. Nemoto, Prog. Theor. Phys. **62**, 1274 (1979).